Efficient bifacial monolithic perovskite/silicon tandem solar cells via bandgap engineering

Published Version:
De Bastiani, M., Mirabelli, A.J., Hou, Y.i., Gota, F., Aydin, E., Allen, T.G., et al. (2021). Efficient bifacial monolithic perovskite/silicon tandem solar cells via bandgap engineering. NATURE ENERGY, 6(2), 167-175 [10.1038/s41560-020-00756-8].

Availability:
This version is available at: https://hdl.handle.net/11585/791330 since: 2021-01-26

Published:
DOI: http://doi.org/10.1038/s41560-020-00756-8

Efficient bifacial monolithic perovskite/silicon tandem solar cells via bandgap engineering

Michele De Bastiani,[1,†] Alessandro J. Mirabelli,[1,2,†] Yi Hou,[3,†] Fabrizio Gota,[4] Erkan Aydin,[1] Thomas G. Allen,[1] Joel Troughton,[1] Anand S. Subbiah,[1] Furkan H. Isikgor,[1] Jiang Liu,[1] Lujia Xu,[1] Bin Chen,[3] Emmanuel Van Kerschaver,[1] Derya Baran,[1] Beatrice Fraboni,[2] Michael F. Salvador,[1] Ulrich W. Paetzold,[4,5] Edward H. Sargent,[3,] and Stefaan De Wolf[1,*]*

1 KAUST Solar Center (KSC), Physical Sciences and Engineering Division (PSE), King Abdullah University of Science and Technology (KAUST), Thuwal 23955-6900, Kingdom of Saudi Arabia.
2 Current affiliation: Department of Physics and Astronomy, Alma Mater Studiorum – University of Bologna, Viale Berti Pichat 6/2, 40127 Bologna, Italy.
3 Department of Electrical and Computer Engineering, University of Toronto, Toronto, Ontario M5S 1A4, Canada.
4 Institute of Microstructure Technology, Karlsruhe Institute of Technology, Hermann-von-Helmoltz-Platz 1, 76344, Eggenstein- Leopoldshafen Germany.
5 Light Technology Institute, Karlsruhe Institute of Technology, Engesserstrasse 13, 76131, Karlsruhe Germany.

Abstract

Bifacial monolithic perovskite/silicon tandem solar cells exploit albedo – the diffuse reflected light from the environment – to increase their performance above that of monofacial perovskite/silicon tandems. Here, we report bifacial tandems with certified power conversion efficiencies (PCEs) > 25% under monofacial AM1.5G 1-sun illumination, that reach power-generation densities (PGDs) as high as ~26 mW/cm^2 under outdoor testing. We further investigate the perovskite bandgap required to attain optimized current-matching under a variety of realistic illumination and albedo conditions. We then compare the properties of these bifacial tandems exposed to different albedos and provide energy yield calculations for two locations with different environmental conditions. Finally, we present an outdoor test-field comparison of monofacial and bifacial perovskite/silicon tandems to demonstrate the added value of tandem bifaciality for locations with albedos of practical relevance.

Main

Globally, an immense research effort is underway aimed at improving further the power conversion efficiencies (PCEs) of perovskite-based photovoltaics (PV).[1] Recent progress in perovskite-based PV is founded on the remarkable optoelectronic properties of perovskites, as well as on important advances made in materials and device engineering, such as the formulation of stable compounds and bulk and surface defect passivation strategies.[2,3] Thanks to their high absorption coefficient, tunable bandgap and remarkable defect tolerance, perovskites are also attractive for realizing efficient multi-junction, tandem devices.[4] The combination of perovskites with market-dominant crystalline silicon (c-Si) solar cells as a bottom cell technology is particularly attractive, since such tandems may increase the PCE of c-Si PV to values higher than its single-junction thermodynamic limit;[4] PCE is a key driver of low levelized cost of electricity (LCOE) at the PV-system level.[5]

Perovskite/c-Si tandem research was initially focused on stacked, four-terminal (4T) tandems owing to the simpler fabrication process.[6-8] However, recent advances in device processing have enabled the two-terminal (2T) architecture, whose optical advantages have enabled the highest PCE for perovskite/c-Si tandems.[9-11] For the latest record performance, a front-flat c-Si cell was used; however, from both a cost and efficiency perspective, it is advantageous to use double-side textured c-Si cells.[12,13] Despite this recent progress, further improvements in performance are necessary to push perovskite/c-Si tandems towards market readiness.

Bifaciality offers further increases in the energy yield of c-Si PV, and can be easily implemented using silicon heterojunction (SHJ) technology by replacing the opaque rear metal contact with grid metallization.[5] As the rear-side of the cell is transparent, reflected and scattered light from the surroundings (*i.e.* albedo) contributes to power generation.[14] For optimized single-junction devices, the generated device current increases linearly with the albedo.

Calculations have shown that perovskite/c-Si tandems can also benefit from bifaciality.[15-18] ~~Coletti *et al.*~~Indeed, recent works have recently explored this for 4T tandems, which offer a relatively easily implementable testing platform.[19] However, in the monolithic configuration, bifacial tandems require judicious re-engineering of the perovskite bandgap for this purpose. As shown in ~~the~~ provious calculations ~~by Onno *et al.*~~,[16,20] as top and bottom cells feature larger and smaller bandgaps respectively, the albedo will only increase the current generated in the bottom cell. In tandems optimized for monofacial use, this may lead to tandem-current mismatch and so a reduction in PCE, which can have a drastic impact on the system-level performance ~~as Dupré *et al.* predicted~~.[17] Therefore, as for conventional current-matching optimizations, the effect of the albedo should be accounted for by adjusting the thickness and bandgap of the perovskite top cell.[15-17,21,22]

Monofacial perovskite/c-Si tandems require a perovskite bandgap close to 1.7 eV,[23] which can be achieved by increasing the bromide-to-iodide ratio in the perovskite crystal.[24] However, this may result in phase segregation under prolonged light exposure, leading to device degradation.[25] Here we show that efficient bifacial tandems, in agreement with recent theoretical predictions, require a narrower perovskite bandgap to achieve current-matching, with a close to pure-iodide composition, thereby improving the operational stability of tandems and increasing their energy yield.

Commentato [TG1]: We try to avoid naming individual researchers when citing their papers. Could you please revise the text accordingly?

Commentato [MDB2R1]: We revised the text and remove all naming references

Perovskite/silicon bifacial tandems

In the field, solar photons that strike the rear side of the device mainly originate from three sources: direct and diffuse sunlight reflected off the ground and surroundings, as well as diffuse sunlight scattered in the atmosphere (Fig. 1a). Direct and diffuse light reflected by the ground is commonly referred to as *albedo* (adimensional); we use the term *rear irradiance* (in units of mW/cm^2) to refer to artificial rear-side illumination in the lab, which we use to study bifaciality. To characterize the performance of tandems, we use PCE (%) for measurements at standard test condition (*i.e*., under monofacial standard test conditions, AM1.5G spectrum, 1-Sun front-side illumination), and power generation density (PGD, in mW/cm^2) for measurements under STC with additional rear irradiance and test field measurements. When referring to the PGD at a specific rear irradiance, we use the bificiality factor (BiFi), to indicate the intensity of the rear irradiance (*i.e.* $PGD_{BiFi\ 200}$ 26, means 26 mW/cm^2 with 200 W/m^2 of rear irradiance)

To understand the impact of albedo on the performance of bifacial perovskite/c-Si tandems, we developed such devices with different perovskite bandgaps. Our tandem layout consists of a both-sides textured silicon heterojunction (SHJ) bottom cell, onto which the perovskite top cell is deposited by solution processing in the *p-i-n* configuration (implying electrons are collected at the sunward side). Figures 1b and 1c sketch this tandem and show a cross-sectional scanning electron micrograph (SEM), respectively. To increase the bifaciality, the SHJ rear contact was optimized to combine minimized series resistance and maximal albedo coupling into the c-Si cell (Fig. 1d).

Commentato [TG3]: Please provide three or four section headings in the main text.

These should relate to the content of the article rather than being generic (ie, avoid Results, although it is fine to use Introduction and Conclusions/Discussion). Headings should be no longer than 60 characters (including spaces) and should not use punctuation.

Commentato [MDB4R3]: The main text is divided with three headings:
Perovskite/silicon bifacial tandems
Optical analysis
Outdoor data and field-test performances
Introduction and conclusions do not have headings

We experimentally fabricated bifacial perovskite/c-Si tandems with five different perovskite bandgaps (1.59, 1.62, 1.65, 1.68, and 1.7 eV; values determined from photoluminescence spectroscopy, Fig. S1) by altering the iodide-to-bromide ratio. Fig. 1e and Table S1 show the statistical distribution of the PV parameters for the tandem cells with different perovskite bandgaps, measured under monofacial STC conditions. As expected, the wider the perovskite bandgap, the larger the open circuit voltage (V_{oc}) of the tandems. J_{sc_tandem} reaches a maximum at a perovskite bandgap of 1.68 eV, corresponding to optimal current matching between the subcells of the tandems discussed here, and resulting in an independently-certified PCE of 25.2% under STC conditions (Fig. S2). Perovskite bandgaps smaller than 1.68 eV result in a lower overall J_{sc_tandem}, as the c-Si sub-cell becomes current-limiting. Similarly, perovskite bandgaps larger than 1.68 eV also result in a lower overall J_{sc_tandem}, as now the perovskite sub-cell becomes current-limiting. The fill factor is slightly higher under silicon-limited conditions than under perovskite-limited conditions, which is in agreement with other reports.[26,27] Overall, the PCE under STC conditions remains close to 25% for tandems with perovskite bandgaps of 1.65, 1.68, and 1.7 eV.

To investigate experimentally the role of rear irradiance, we measured the bifacial tandems by placing them between two solar simulators. The front illumination (perovskite-side) was kept at 1-Sun (100 mW/cm^2), whereas the device rear (silicon-side) was illuminated with intensities ranging from 0 to ~95 mW/cm^2 (*i.e.* 0.95 Suns equivalent); Fig. S3 shows the detailed characterization set-up. To facilitate contacting and prevent cell degradation during the experiment, the devices were vacuum-laminated between two sheets of glass, using butyl rubber as edge-sealant. Here, we note that we used single-lamp solar simulators for practical convenience; these simulators are not ideal for the tandem configuration as their spectra vary somewhat from the AM1.5G spectrum (see Fig. S3 for more details).[28]

Fig. 1f compares the J-V curves of a bifacial tandem (perovskite bandgap of 1.62 eV), before encapsulation measured with an LED-based solar simulator (yellow) and after encapsulation measured with the bifacial setup without rear irradiation (red). For the latter, the reduction in the J_{sc} (1-1.5 mA/cm^2) is caused both by the glass-encapsulation, (front glass reflection and suboptimal refractive-index matching of the glass/vacuum/top-electrode stack that increases the reflection losses), but also by the different frontside solar simulator used in the bifacial setup (Fig. S3). Fig. 1f also shows that the bifacial tandem (1.62 eV-yellow) generates a slightly lower current (~0.5 mA/cm^2) in monofacial operation mode, when compared with an opaque metal rear-electrode; the latter aiding internal light trapping in the c-Si cell (1.68 eV-blue).[29] However, in the presence of 20 mW/cm^2 rear irradiance (orange), J_{sc_tandem} clearly surpasses its monofacial counterparts. Here we underline that such an albedo is realistic for industrial solar parks optimized to operate with bifacial modules. In the near future it is likely that albedos resulting in rear irradiances as high as 30 mW/cm^2 can be achieved, *e.g.* with the implementation of a reflective coating covering the ground and proper site selection.[30]

Commentato [TG5]: This paragraph is quite long. We suggest you to break it into more paragraphs to improve readability.

Commentato [MDB6R5]: We split the paragraph, separating fig. 1f, 1g, and 1h. The paragraph of fig. 1g describe the key concepts of the bifacial experiments in a concise way, despite its length (35 lines)

To thoroughly explore the bifacial configuration, in Fig. 1g we explore the change in device performance as a function of rear irradiance, ranging from 0 to ~95 mW/cm^2, of encapsulated bifacial tandems with different perovskite bandgaps. In general, the tandem V_{oc} slightly increases with rear irradiance by around 20 mV, as expected, given the higher density of photo-generated charge carriers in the bottom cell. However, J_{sc_tandem} is the parameter that benefits most from the presence of albedo. As the rear irradiance increases, J_{sc_tandem} rises rapidly, plateauing at ~20 mW/cm^2 of rear irradiance, for most bandgaps tested. The enhancement in J_{sc_tandem} with rear irradiance is most pronounced for the narrower bandgap perovskites tested (1.59, 1.62 eV). The reason is that both sub cells simultaneously generate more current: the perovskite top cell due its smaller bandgap, and the c-Si bottom cell due to the rear irradiance. Both experimental and calculated data show that with decreasing bandgaps, the rear irradiance required to achieve current-matching slightly increases. The effect of albedo on the FF is more complex. For all band gaps, the FF slightly drops as the rear irradiance increases from 0 to 20 mW/cm^2 before partially recovering at irradiations higher than ~20 mW/cm^2. A similar correlation between FF and current-matching conditions is well known for monofacial tandems when spectrally changing the incident solar radiation, as recently show by Köhnen *et al.* and Boccard *et al*.[26,27] For a detailed explanation of this phenomenon, we refer the reader to Section S4. As demonstrated in Fig. 1g and Table S1, J_{sc} strongly increases with stronger rear irradiance up to values around 10-20 mW/cm^2, which empirically demonstrates the extent to which the tandems tested under monofacial, STC condictions are current limited by the c-Si bottom cell. Along with improved current matching, the FF slightly decreases, as previously shown from basic two-diode considerations (see also Fig. S4c). For a rear irradiance exceeding 20 mW/cm^2, the tandems enter the regime of current limitation by the perovskite top cell as no further enhancement in J_{sc} is observed with increasing rear irradiance. For this regime, the tandem again shows a slightly increased FF. As stated earlier, in the presence of albedo, we use PGD (in mW/cm^2) rather than PCE (%) to indicate the performance of bifacial tandems. Similar to the J_{sc} trend, the PGD of the bifacial tandem strongly benefits from the addition of rear irradiance, achieving values as high as ~28 mW/cm^2 for perovskites with band gaps of 1.59 and 1.62 eV (with ~95 mW/cm^2 of rear irradiance: $PGD_{BiFi950}$ 27.85 mW/cm^2). Notably, our measurements show that a rear irradiance of 30 mW/cm^2 can improve the absolute PGD of a bifacial tandem (with 1.59 eV perovskite top cell) by more than 25% with respect to its monofacial configuration (see Fig. S5 for more details). Such an albedo is realistic in solar fields, where snow, sand or concrete may cover the ground surface.[22,31] When compared with monofacial perovskite/c-Si tandems, this enhancement in power output favors bifacial technology over several monofacial configurations, as shown in Table S3, underlining the potential of this technology.

To test our findings, we analyzed the enhancement in PGD for a batch of 29 bifacial tandem cells (with a perovskite bandgap of 1.59 eV), with and without 30 mW/cm^2 of rear irradiance (Fig. 1h; PGD_{BiFi0} blue, $PGD_{BiFi300}$ yellow). Without albedo, the devices show a distribution of PGD_{BiFi0} centered at 21.5 mW/cm^2. Conversely, with an rear irradiance of 30 mW/cm^2 the overall $PGD_{BiFi300}$ increases, and the average shifts to 25.5 mW/cm^2, an absolute increase of 19 % in power generation.

Formattato: Rientro: Prima riga: 1,27 cm

With rear irradiance, the operating temperature of the tandem is increased. In Fig. S6, we investigate the temperature variation under different rear irradiance conditions alongside their relative cooling relaxation times. Based on these cooling times, we established a minimum time-interval between the sequential measurements carried out in the lab for Fig. 1g, in order to ensure a cell temperature close to STC conditions. However, the outdoor operational temperature of a solar cell (especially in a sunny and hot climates) can reach 50 °C and more (Fig. S7), even for perovskite/c-Si tandems where thermalization losses are significantly reduced compared to single-junction devices.

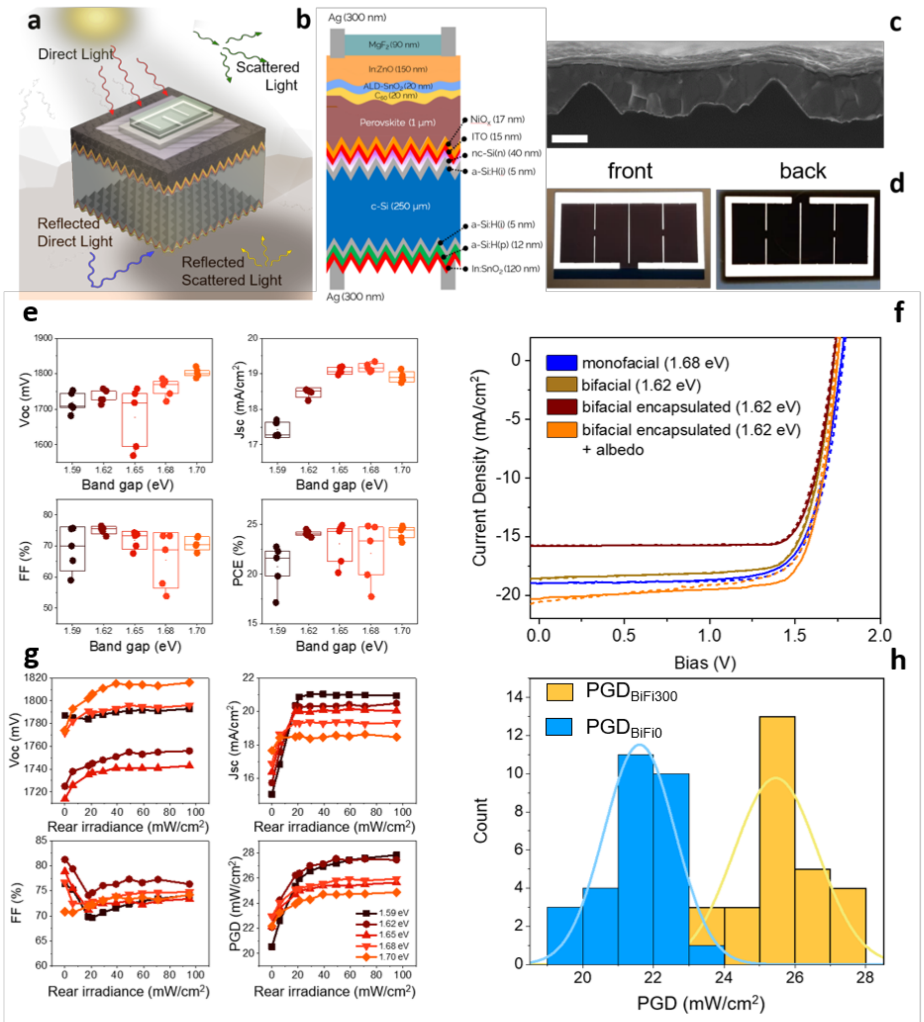

Fig. 1. Perovskite/silicon bifacial tandems. (a) Sketch of light absorption in a bifacial perovskite/c-Si tandem, featuring albedo. (b) Cross-sectional sketch of the perovskite/c-Si bifacial tandem. (c) Cross-section SEM micrograph of the tandem realized on both-sides textured c-Si bottom cell, white scale bar: 1 μm. (d) Picture of the front and rear contact of the device. (e) Photovoltaic performance for bifacial tandems with different perovskite bandgaps, measured only with front light ~~(1 Sun)~~(including: minimum, maximum ticks; median, lower quartile, and upper quartile in the box plot). (f) Comparison of the J-V curves of a monofacial tandem (blue) and a bifacial tandem (dark yellow) measured using an LED-based solar simulator. The same bifacial device encapsulated and measured in the bifacial setup with front light only (red) and front light plus rear irradiance (orange). Solid line: reverse voltage scan direction. Dashed line: forward voltage scan direction (g) Photovoltaic performance of bifacial

Commentato [TG7]: Could you please define all features – square, box lines, and ticks – of box-and-whisker plots?

Commentato [MDB8R7]: Included

Commentato [TG9]: Could you please specify what the dashed and solid curves refer to?

Commentato [MDB10R9]: done

tandems with different perovskite bandgap, as a function of the rear irradiance. (h) Statistical distribution of the power generation of 29 tandems measured with (yellow, BiFi300) and without (blue, BiFi0) rear irradiance. The fits are included as a guide for the eye.

Optical analysis

To further understand current-matching conditions for bifacial tandems, we collected external quantum efficiency spectra (EQEs) for the devices with different perovskite bandgaps (Fig. 2a). By integrating the EQE-weighted solar spectrum, we can extract the current-matching condition (for the monofacial tandem case), which is achieved for a perovskite bandgap between 1.68 eV and 1.7 eV, in agreement with the trend for J_{sc} shown in Fig. 1e. To visualize the influence of the bandgap of the perovskite on J_{sc_tandem}, Fig. 2b plots the integrated currents derived from the EQEs in Fig. 2a (closed circles) for both the perovskite (red) and silicon (blue) sub-cells *vs.* the perovskite bandgap; we note that altering the perovskite bandgap does not notably alter its refractive index, and therefore the overall reflection of the tandem (Fig. S9). We further compare these currents with those obtained from *J-V* measurements (Fig. 1g), hollow circles for bifacial devices with ~95 mW/cm^2 rear irradiance (red) and without effective-albedo (blue). Fig. 2b again demonstrates that while a 1.7 eV perovskite bandgap is optimal for monofacial tandems, in the bifacial configuration this offers little to no gain in current. For small bandgaps (*e.g.* 1.59 eV, Fig. 3b), the 1-Sun integrated EQE shows a remarkable mismatch in current, due to a current limiting c-Si sub-cell. However, while this is disadvantageous in a monofacial configuration, it enables the highest current gain in the bifacial configuration, provided that sufficient rear irradiance is available.

Commentato [TG11]: Could you please describe the blue and yellow curves as fits or guides to the eye (details about the fit should be provided, if relevant)?

Commentato [MDB12R11]: We included the fit as a guide for the eye

Commentato [MDB13]: Second heading

ha formattato: Tipo di carattere: Grassetto

To further analyze possible loss mechanisms due to optical effects as a function of the layer stack, we performed optical simulations. Fig. 2c and Fig. 2d show the front and rear side absorptance, respectively, considering the layers of the stack of Fig. 1b for a perovskite bandgap of 1.68 eV (see Fig. S10 for details). The indium zinc oxide (IZO) and fullerene (C_{60}) top layers cause significant parasitic absorption in the UV regime. Moreover, the IZO layer also induces losses due to free carrier absorption between 800 and 1100 nm, a range where the c-Si bottom features a high quantum efficiency, affecting thus significantly the current output. Overall, under AM1.5G 1-Sun illumination, parasitic absorption and reflection losses translate into J_{sc} losses of 4.6 mA/cm^2 and 3.1 mA/cm^2, respectively; IR light transmission results in another 0.9 mA/cm^2 in J_{sc} loss. Photons impinging on the bifacial tandem rear can only be absorber by the c-Si bottom cell. Here, high energy photons could be parasitically absorbed in the rear-contact stack of the SHJ cell. The 2-side textured c-Si wafer aids in geometric light trapping, reducing reflection losses in the 600 - 1000 nm wavelength range. For wavelengths around 500 nm a significant reflection loss is apparent resulting in imperfect light incoupling in these prototypes with the given rear-contact layer stack. Future work can address this loss by optimizing the refractive index combination in the rear stack and thereby enhancing the light incoupling from the rear side. Finally, we extended our simulation to the encapsulated device (see Fig. S11), which, as experiments already showed, suffers from slightly increased reflection losses.

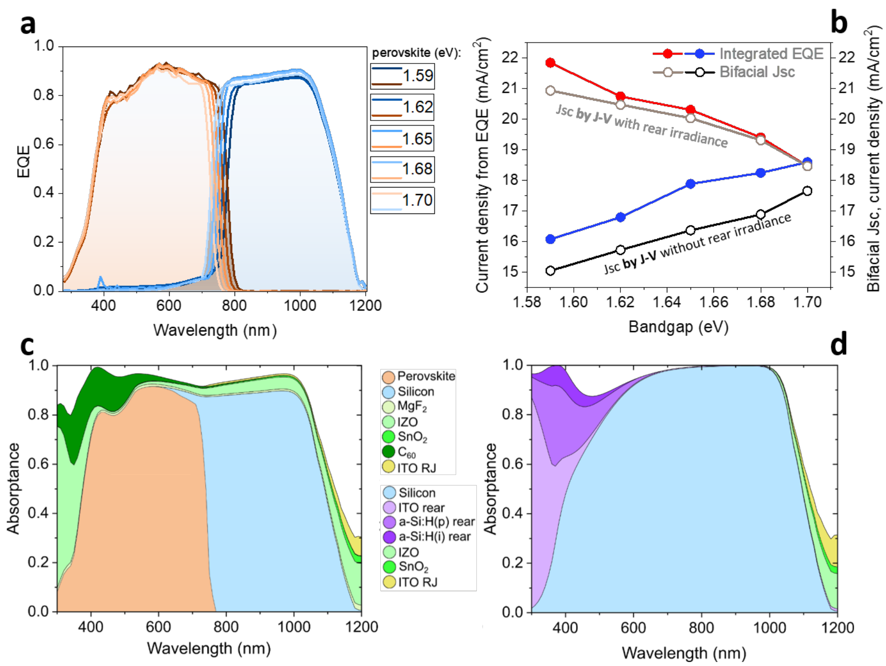

Fig. ~~3~~2. Optical analysis. (a) EQEs of the bifacial tandems with different bandgap. The orange lines correspond to the EQE of the perovskite top cell; the blue lines correspond to the EQE of the silicon bottom cells~~.~~. (b) Comparison between integrated EQE current density and Jsc from J-V curves. Note that the EQE measurements were performed without encapsulation, but the J-V measurements were done with encapsulation, which lowers the J_{SC} compared to EQE values. Full dots: integrated EQE current density for the perovskite (red) and c-Si (blue), as a function of the perovskite bandgap. Hollow circles: J_{sc} of the bifacial device without rear irradiance (black) and with rear irradiance (gray, ~95 mW/cm^2), as a function of the perovskite bandgap, extrapolated from Fig. 2c. (c) Front and (d) rear side absorption of the layers composing the bifacial tandem with a perovskite bandgap of 1.68 eV.

Outdoor data and f~~F~~ield-test performances

To further test the potential of the technology, we compared the outdoor performance of monofacial and bifacial tandem devices under three different specific albedo conditions: concrete, synthetic grass, and a white background. We installed the monofacial and the bifacial devices in our outdoor test field on the KAUST campus and changed the ground material to

Commentato [TG14]: Could you please make clear in the caption or in the figure legend what the orange and blue curves refer to?

To improve the figure readability, it might be better if the legend is moved outside the plot and the boxes from each portion are removed.

Commentato [MDB15R14]: Fig 2a is improved and the caption modified accordingly

Commentato [TG16]: Could you please specify in the label axis and in the legend that Integrated EQE refers to a current density?

Commentato [MDB17R16]: Fig 2b is modified, we accepted the changes in the caption

Commentato [TG18]: Correct?

Commentato [MDB19]: Third heading

simulate these different albedo conditions (see Fig. S12 for more details, including the reflectance data from these surfaces). In this way, the performance relies on albedo rather than rear irradiance.

For each condition, we recorded the J-V characteristic with a time interval of 10 min during a measurement time of one hour. To achieve maximum consistency, we carried out the experiments at peak sun hours, using a pyranometer and a calibrated c-Si solar cell to monitor the light intensity. Fig. 3a shows the PGD and the J_{sc} of the bifacial (black) and monofacial (red) tandem devices. Both devices consist of the same layer stack apart from the rear electrode (opaque *vs.* transparent electrode) and perovskite bandgaps. The bifacial tandem outperforms its monofacial counterpart for every albedo condition. The gain in performance was particularly striking when using concrete as the ground, where the bifacial tandem achieved a remarkable PGD of 25.9 mW/cm^2. The increase in power output can be mainly attributed to the higher currents generated in the bifacial configuration. Overall, the average increase in bifacial power output was 20% for concrete, 6% for a white background, and 4.3% for synthetic grass. We note that certain materials such as snow have typically an even larger albedo than concrete.

We extended the comparison between monofacial and bifacial tandems to two test-field locations: Jeddah – Saudi Arabia, representing hot and sunny environments; and Karlsruhe – Germany, representing a typical moderate climate. Fig. 3b shows the PGD of the bifacial tandems, from dawn (06.00 am) to dusk (06.00 pm), measured at 10 minutes intervals, over five days of investigation. To highlight the different irradiation conditions, we did not normalize the output power density to Sun equivalents, but rather reported the Sun's intensity, obtained through a pyranometer and a calibrated c-Si reference cell. For the experiment, the cells were placed on a test-field structure, with similar orientation and distance from the ground, consisting of bright sand and concrete (Jeddah), and concrete (Karlsruhe). In both sites, the bifacial tandem performed significantly better than the monofacial one, particularly, during midday when the light intensity is close to 100 mW/cm^2 (Jeddah) or 80 mW/cm^2 (Karlsruhe). Furthermore, the Karlsruhe data reveals that the enhancement in PGD is more pronounced on sunny days (day 1, 2), which predominantly exhibit direct radiation compared to cloudy days with mostly diffuse irradiation (day 3, 4, 5).

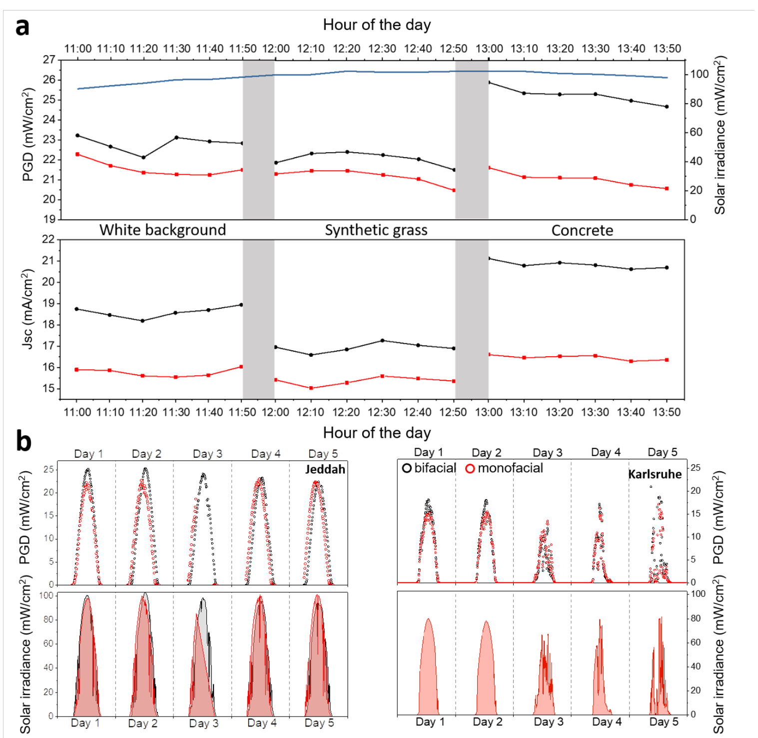

Fig. 3. Outdoor testing of bifacial tandems. (a) Comparison of PGD and J_{sc} for bifacial (black) and monofacial (red) tandems with different albedo conditions: concrete, styrofoam, and grass. The perovskite bandgaps are 1.62 eV and 1.68 eV for the bifacial and monofacial tandems, respectively. For each point, ~~T~~the ~~performances~~ current

Commentato [TG20]: Can you please describe the two different labels used for the X-axis (i.e. day time on top and the 0-50 range at the bottom)?

Commentato [MDB21R20]: We revised Fig 3a and use the same X-axis, top and bottom. In the previous version the bottom axis was in minutes.

density and therefore the PGD are normalized with the respective ~~Sun~~ solar irradiance~~intensity~~ (blue line). The gray areas in the plot represent the operational time to change the setup, from one background to another. (b) Test-field power conversion comparison for bifacial (black) and monofacial (red) tandems, measure over five days in two different locations: Jeddah, Saudia Arabia (22.302494, 39.110737); Karlsruhe, Germany (49.094577, 8.429605). For the Jeddah experiment, the devices were placed in the test-field in different times, therefore we reported the intensity of the solar irradiance (red for monofacial, and black for bifacial) for each day. For the Karlsruhe experiment, the devices were placed in the test-field at the same time, therefore we reported only a single solar irradiance (red).~~For each day and location we report the intensity of the solar irradiance.~~ For each device, the perovskite bandgap is 1.62 eV.

In Fig. 4a and 4b, we report the analysis of performances of the bifacial (4a) and monofacial (4b) tandems with respect to the solar irradiance from the five days of field data collected from the Jeddah location. Since the data are collected under different solar irradiations, we normalized the J_{sc_tandem} and the PGD for direct comparison. For the J_{sc_tandem}, the trend of the monofacial tandem is linear. Conversely, for the bifacial tandem the current shows some hysteresis with the solar irradiance, showing sub-linear behavior during the morning (from 06:00 am to 12:00 pm) that becomes linear in the afternoon (from 12:00 pm to 06:00 pm). The scattered data at low irradiance (10-25 mW/cm^2) are an artifact induced by a partial shading of the pyranometer during early mornings and late afternoons (Fig. S13). To understand the behavior of the current in the bifacial tandem, we measured the albedo of our test-field over five consecutive days (Fig. S14). We found that, while the albedo is on an average constant during the week (~0.25), it fluctuates during the day, with lower values in the morning due to partial shading of the ground. This reflects the importance of controlling the albedo to maximize the performance of the bifacial tandem. The trend of the V_{oc} is similar for both devices, where the voltage reaches a constant value at solar irradiances of 15-20 mW/cm^2. The FF shows a narrower distribution for the bifacial device, particularly at low solar irradiance, without evident differences between the morning and the afternoon. Interestingly, for the

Commentato [TG22]: Could you please provide further details?

Commentato [MDB23R22]: The whole experiment lasted for three hours outdoor, during this time the intensity of the Sun changed (blue line). To be able to precisely compare the different conditions of albedo, we normalized the current (and then the PGD) to the Sun intensity.

Commentato [TG24]: Why the Jeddah location has both a bifacial (black) and monofacial (red) related irradiance while the Karlsruhe one does not?

Commentato [MDB25R24]: For Karlsruhe the two devices were installed simultaneously, therefore they were exposed to the same solar irradiance. We clarified this in our response letter after the first revision.

To better clarify this point, we modified the caption accordingly.

bifacial tandem, the normalized PGD reflects the effect of the lower current during the morning, to improve in the afternoon. Overall, the normalized PGD distribution is similar for the two devices over the day.

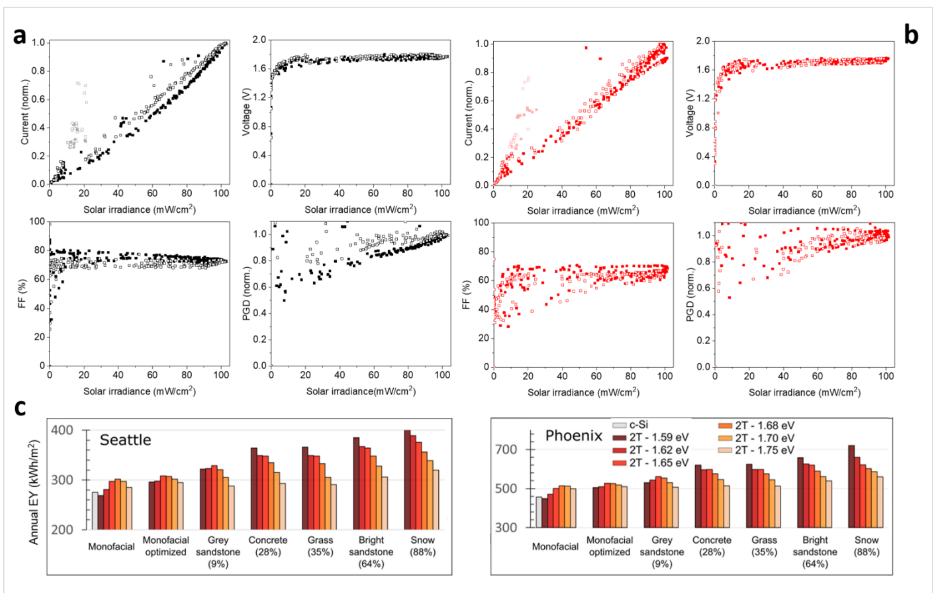

Fig. 4. Test-field analysis and energy yield. J_{sc_tandem}, V_{oc}, FF, and PGD versus to the solar irradiance for the bifacial (a) and monofacial (b) tandems of Fig. 3b. For the J_{sc} and PGD the data are normalized to allow the comparison. The full squares refer to data collected in the morning (06:00am – 12:00pm), the open squares to data collected in the afternoon (12:00pm – 06:00pm). (c) Energy yield calculations for monofacial and bifacial tandems with different perovskite bandgaps and under different albedo conditions, compared with a c-Si solar cell, for two locations: Seattle and Phoenix.

Commentato [TG26]: Is this correct?

Commentato [MDB27R26]: correct

Finally, we performed energy yield simulations to assess the performance of bifacial tandems under realistic outdoor conditions (see results in Fig. 4c). Two locations, Phoenix and Seattle, have been chosen to represent two very different climatic conditions. Moreover, the annual energy yield was computed for different perovskite bandgaps and albedo conditions (see Section S15 for more details). The highest monofacial energy yield is achieved with a perovskite bandgap of 1.68 eV and 1.65 eV for both locations, using the identical layer stack of the bifacial architecture and an optimized perovskite thickness, respectively. Despite not featuring an ideal bandgap for monofacial tandems (between 1.70 eV and 1.80 eV), this bandgap results in the most optimal current matching throughout the whole year for a 1000 nm thick perovskite layer and thus achieves the highest energy yield. The lowest monofacial performance occurs for the smallest bandgap (1.59 eV), due to significant current-mismatch losses. The scenario changes significantly for the bifacial configuration. Even in the presence of a ground with a reflectivity as low as dark concrete (average albedo reflectivity equal to 28%), the optimum bandgap shifts to lower values: in Seattle, which represents a temperate climate, as well as in Phoenix, which represents a sunny, desert climate, it is 1.59 eV, due to the larger share of direct sunlight, resulting in a stronger rear irradiance. Notably, bifacial energy yield improvements of around 32% in Seattle and 37% in Phoenix (relative to the best monofacial tandems with optimized layers thicknesses and a bandgap of 1.65 eV) are computed with a bandgap of 1.59 eV for the perovskite and the most reflective ground. Materials with high reflectivity could be used to enhance the albedo in locations with a high share of direct irradiation, to fully exploit the potential of bifacial perovskite/c-Si tandems with narrow perovskite bandgaps. It should be noted that in order to maintain generality, the energy yield calculations provided in Figure 4c do not consider installation specific aspects such as self-shading of the module or shading due to adjacent modules. However as shown in Fig. S16 and Fig. S17, the key trends presented are valid for representative installation scenarios that would consider such shading.

Commentato [TG28]: Folowing the concerns raised by Reviewer #1, could you please be more explicit that this might means the numbers are overestimated?

Conclusions

We have experimentally shown how bifaciality can be used to enhance the performance of monolithic perovskite/c-Si tandems. The device configuration with a transparent back electrode relies on the albedo to enhance the current generation in the bottom cell, while simultaneously enhancing the current generation in the perovskite top cell, thanks to a narrower perovskite bandgap. This matching is achieved for a 1.59-1.62 eV bandgap perovskite, where the bromide content is minimized, thereby strongly reducing the stability issues related to halide segregation. We evaluated the bifacial tandem performance in test-field experiments and we predicted the energy yield for bifacial and monofacial tandem configurations in different climates. In both cases, the bifacial tandem outperformed the monofacial configuration, validating the promise of this technology. This work demonstrates the potential for a new class of efficient solar cells, which can close the gap with the 30 mW/cm^2 power generation density barrier, for a highly performant and affordable technology. From here, further improvements in device performance and scaling-up of the technology are logical next steps, bringing this technology closer to the PV market.

Methods

Device Fabrication: Silicon heterojunction bottom cells are fabricated on float-zone double side-textured four inches wafers (TOPSIL, n-doped, resistivity 1-5 ohm/cm, and thickness 250-280 mum). The wafers are processed with alkaline solution to obtained random pyramids texturing. After the wafers are cleaned in RCA1 and RCA2 solutions and dipped in hydrofluoric acid to remove the silicon oxide layer. The intrinsic I (5 nm) and doped amorphous and nanocrystalline layers (p, n 12 nm and 40 nm respectively) are deposited via plasma enhanced chemical vapour deposition (PECVD) in an Octopus2 cluster (Indeotec). The ITO rear contact (100 nm) and the recombination junction (15nm) are sputtered in the physical vapour deposition (PVD) part of the Octopus2 cluster with base pressure 1 x 10^{-5} Torr, 13.56 Mhz RF source, 0.9 W/cm^2 power density, in an Ar/O_2 atmosphere (0.8% O_2 content) and a process pressure is 1 x 10^{-3} Torr (ITO target from Vital Thin Film materials – 97% In_2O_3 3% SnO_2).

After the PVD deposition the bottom cells are annealed 5 min at 200 °C. For the top cell, NiOx (17 nm, Plasmaterials) is sputtered (Angstrom EvoVac) at base pressure of < 1 x 10^{-6} Torr in pure Ar atmosphere with no intentional heating or cooling of the substrate, at a power density 1.97 W/cm^2 and 13.56 MHz RF source.[32] Prior to the perovskite deposition the NiOx layer is passivated with 4-bromobenzoic acid (Sigma Aldrich). The process is done by spin casting of 2 mg/ml 4-bromobenzoic acid in ethanol. After spin casting the films were annealed at 90 °C and after cooling down washed with ethanol for several times.. The triple cation perovskite solution (1.68 M) is prepared in a 4:1 Dimethylformamide Dimethyl sulfoxide (DMF:DMSO, Sigma Aldrich) using 36.4 mg of caesium iodide (CsI, Alfa Aesar), 44,8 mg of methyalmmonium bromide (MABr, Greatcell), 389 mg of fomamidinium iodide (FAI, Greatcell), lead bromide ($PbBr_2$, Sigma Aldrich) and lead iodide (PbI_2, Alfa Aesar). The solution was stirred until complete dissolution of the precursors. The PbI_2 and $PbBr_2$ amount varied according to the desired bandgap. For the perovskite film formation, the perovskite precursors is spin coated on the bottom cell substrate with a three-steps process: initially 600 rpm, then 2000 rpm, finally 7000 rpm. During the acceleration between the second and third step, anisole is dripped as solvent quencher. Finally, the devices are annealed in nitrogen at 100 °C for 15 min. On top of the perovskite, lithium fluoride LiF (1 nm Alfa Aesar) and C_{60} (20 nm, NanoC) are thermally evaporated as electron transport layer (Angstrom EvoVac). A layer of 20 nm of tin oxide (SnOx Tetrakis(dimethylamino)tin and H_20 as precursors, with N_2 as the gas carrier) deposited via atomic layer deposition (ALD, Picosun) is used as protective buffer layer. As top electrode, 110 nm of indium zinc oxide are sputtered in an Angstrom EvoVac sputtering system (base pressure < 1 x 10-6 Torr) with RF power of 42 W (90% In_2O_3/ 10% ZnO, 99.9% Plasmaterials). To functionally contact the top and bottom transparent electrodes, we thermally evaporated (Angstrom EvoVac) 350 nm of silver contacts (base pressure 1 x 10^{-6} Torr), on the front and afterwards on the rear of the tandem using an aperture mask. Lastly, 95 nm of MgF_2 as antireflection film are thermally evaporated (Angstrom EvoVac) on top of the bifacial device.

Device Characterization: To evaluate the performances of the tandems without rear irradiance, we used a calibrated Wavelabs Sinus 220 LED based solar simulator with AM 1.5G irradiance spectrum as our light source and we coupled it with a Kiethley 2400 series SourceMeter to take the J-V measurements. The data is recorded via a homemade MATLAB based software. The solar cells are measured from -0.1 V to + 1.9 V at 200 mV/s in both forward and reverse scan directions and the illuminated area, defined by a laser cut shadow mask, is 1.03 cm^2. EQE measurements are performed using PV-Tools LOANA equipment. For the rear irradiance setup we used a Abet Technologies Sun 3000 Class AAA and a Newport Oriel Sol3A Class AAA, both Xenon (Xe) arc lamp based. For the rear irradiance measurements, the stability test, and the field-test investigation, we encapsulated the bifacial tandem with a vacuum laminator (Ecolam 5 Ecoprogetti) using glass and ~~butyl rubber~~10 mm wide and 1 mm thick butyl rubber Solargain® edge sealant with desiccant (Quanex, SET LP03).~~.~~

Commentato [MDB29]: Included

Test field experiment: For the field-test, we used an I-V tracer from EKO (model MP-160). The I-V characteristics of multiple samples are probed successively using the multiplexers MI-520 again from EKO. Current-voltage curves are acquired with a scan rate of 200 mV/s, and we measured all physical parameters with a time interval of 10 min. The global horizontal irradiance on the plane of the devices is measured using the pyranometer MS-802 (EKO), mounted on the same structure as the devices. The solar cells are mounted on a structure with a tilt angle of 25 degrees and South orientation, located in KAUST's outdoor testing field on the KAUST campus, near the village of Thuwal (Saudi Arabia; 22.302494, 39.110737). Furthermore**,** solar spectra is acquired using the spectrometers QE65PRO (visible spectral region) and NIRQuest512 (NIR spectral region) from Ocean Optics. The spectrometers are built into a temperature-controlled housing, and possess a wavelength resolution of < 2 nm across the entire VIS/NIR. For the field-test in Karlsruhe, we used a Keithley 2600 series SourceMeter to record I-V curves with a time interval of 3 minutes. A homemade LabVIEW program is used to select successively the two solar cells using multiplexers and save the data. Then through a MATLAB code the MPP of each curve is extracted. The solar cells are mounted on a homemade metallic frame with a tilt angle of 45 degrees and South orientation. A calibrated c-Si solar cells mounted next to the bifacial cells is used to extract the Suns, by computing the ratio between the short-circuit current in the test-field for each data point and the short-cicruit current under a solar simulator with AM1.5G irradiance spectrum.

Simulations and Enery Yield Modelling: The optical simulations and energy yield modelling platform are accurately described ~~by Schmager et al~~elsewhere. [33] Here we provide a short description of its main features. The modelling platform combines four modelus together: (i) optics module, (ii) irradiance module, (ii) electrics module and (iv) enrgy yield core module. For the simulations in Fig.2c, Fig.2d and Fig.S6, the optics module alone was used. This module employs a combination of transfer matrix method (TMM) for thin, optically coherent layers and series expansions of Lambert-Beer law for optically thick layers, taking into account multiple reflections at contiguous interfaces. Textured interfaces were handled using geometrical ray tracing, as suggested by Baker-Finch and McIntosh.[34] To model as closely as possible the fabricated devices, complex refrative indeces of most of the layers were measured in-house at KAUST. The output of the module is stored in multi-dimensional matrices, namely the reflectance matrix, the transmittance matrix and the absorptance matrix for each layer in the stack. Each matrix is spectrally and angularly resolved for a discrete number of photon wavelength and incoming angle. Data for normal incidence were used for the optical simulations in Fig.3c, Fig.3d and Fig.S6. For the energy yield simulations, the remaining three modules work together with the optics module. The irradiance module uses typical meteorological year (TMY3) data sets from the National Renewable Energy Laboratory (NREL) to compute angularly and spectrally resolved clear sky irradiance data of hundreds of locations in the USA with a time resolution of one hour, using the 'simple model of atmospheric radiative transfer of sunshine' (SMARTS).[35] [36] Then a simple model is used to account for cloud coverage, in order to obtain realistic direct and diffuse irradiance data.[37] The energy yield core module combines the otput of the irradiance and optics module to compute the light-collected current J_{ph} in the perovskite and silicon sub-cells. In the bifacial configuration, the albedo contribution was computed using reflection data from the ECOSTRESS library [38]. Shading due to the module itself and the other rows of modules was not taken into consideration. Then the electrics module computes the maximum power point calling the circuit simulator LTspice. An equivalent circuit identical to the one in Fig.S2a was used for the simulations of the tandem perovskite/silicon cells. Finally, the energy yield module sums the contributions for each hour of the typical meteorological year and extracts the annual energy yield.

Acknowledgments

This work supported by the King Abdullah University of Science and Technology (KAUST) Office of Sponsored Research (OSR) under award no. OSR-2018-CPF-3669.02, KAUST OSR-CARF URF/1/ 3079-33-01, KAUST OSR-CRG RF/1/3383, ~~and~~ KAUST OSR-CRG2018-3737, and IED OSR-2019-4208. The financial support of the German Federal Ministry for Economic Affairs and Energy (CAPITANO, funding code: 03EE1038B) and the Initiating and Networking funding of the Helmholtz Association (HYIG of U.W.P. (funding code: VH-NG1148); PEROSEED (funding code: ZT-0024); and the Science and Technology of Nanostructures Research Program) is acknowledged. Furthermore, the authors are grateful for the help and support of Dr. Adrian Mertens and Aiman Rozalier from KIT in setting up the outdoor measurements in Karslruhe. The authors acknowledge the support of ABET Technologies and Newport. The authors thank TUV Rheinland Group, Germany, for providing solar spectra from TUV's outdoor test field on the KAUST campus, Thuwal, Saudi Arabia. The authors are grateful for the support of Dr. Justin Lee Mynar~~,~~ and KAUST Corelab ~~Executive Director for the Corelab Laboratories (KAUST)~~, and Dr. Ahmed H. Balawi for the fruitful discussions.

Commentato [MDB30]: Included

Commentato [MDB31]: Revised

Authors information

*stefaan.dewolf@kaust.edu.sa
*ted.sargent@utoronto.ca
†these authors equally contributed

Contributions

M.D.B conceived the idea; M.D.B. and A.J.M. fabricated the devices; Y.H., B.C., and A.S.S. developed the perovskite bandgaps; E.A. developed the tandem top contact and layout; E.A. and F.H.I. developed the tandem hole transport layer; T.G.A. perfomed the tandem simulations; M.D.B, T.G.A., E.V.K. developed the silicon bottom cell; F.G., U.W.P. and L.X. performed the optical modeling; J.L. performed the electrical modeling; M.F.S., F.G., J.T. and J.L. developed the field-test setup; F.G. and U.W.P. performed the energy yield calculations; M.F.S supervised the field-test experiment; M.D.B., M.F.S., A.S.S., F.G., and U.W.P wrote the manuscript; D.B., B.F., E.H.S, and S.D.W. supervised the project.

Data availability

Commentato [TG32]: In the present case, I suggest that you introduce a DAS worded as follows:
"All data generated or analysed during this study are included in the published article and its Supplementary Information."

Commentato [MDB33R32]: Included

All data generated or analysed during this study are included in the published article and its Supplementary Information.

Competing Interests

The authors declare no competing interests.

ha formattato: Tipo di carattere: 10 pt

ha formattato: Tipo di carattere: 9 pt

Commentato [TG34]: Please include a statement that declares any financial and non-financial competing interests you or your co-authors may have. For more details, please see our Competing Interests policy page: http://www.nature.com/authors/policies/competing.html

Commentato [MDB35R34]: Included

ha formattato: Tipo di carattere: Non Grassetto

References

1 NREL. Best-Research cell efficiency chart. (2020).

2 Aydin, E., De Bastiani, M. & De Wolf, S. Defect and contact passivation for perovskite solar cells. *Advanced Materials* **31**, 1900428 (2019).

3 Al-Ashouri, A. *et al.* Conformal monolayer contacts with lossless interfaces for perovskite single junction and monolithic tandem solar cells. *Energy & Environmental Science* **12**, 3356-3369 (2019).

4 Leijtens, T., Bush, K. A., Prasanna, R. & McGehee, M. D. Opportunities and challenges for tandem solar cells using metal halide perovskite semiconductors. *Nature Energy* **3**, 828-838 (2018).

5 Allen, T. G., Bullock, J., Yang, X., Javey, A. & De Wolf, S. Passivating contacts for crystalline silicon solar cells. *Nature Energy*, 1-15 (2019).

6 Aydin, E. *et al.* Zr-Doped Indium Oxide (IZRO) Transparent Electrodes for Perovskite-Based Tandem Solar Cells. *Advanced functional materials* **29**, 1901741 (2019).

7 Dewi, H. A. *et al.* Highly Efficient Semitransparent Perovskite Solar Cells for Four Terminal Perovskite-Silicon Tandems. *ACS applied materials & interfaces* **11**, 34178-34187 (2019).

8 Chen, B. *et al.* Enhanced optical path and electron diffusion length enable high-efficiency perovskite tandems. *Nature Communications* **11**, 1-9 (2020).

9 Chen, B. *et al.* Blade-Coated Perovskites on Textured Silicon for 26%-Efficient Monolithic Perovskite/Silicon Tandem Solar Cells. *Joule* (2020).

10 Elshorbagy, M. H. *et al.* A monolithic nanostructured-perovskite/silicon tandem solar cell: feasibility of light management through geometry and materials selection. *Scientific Reports* **10**, 1-8 (2020).

11 Duong, T. *et al.* High Efficiency Perovskite-Silicon Tandem Solar Cells: Effect of Surface Coating versus Bulk Incorporation of 2D Perovskite. *Advanced Energy Materials*, 1903553 (2020).

12 Hou, Y., Aydin, E., Bastiani, M. D., Wolf, S. D. & Sargent, E. *Science*.

13 Sahli, F. *et al.* Fully textured monolithic perovskite/silicon tandem solar cells with 25.2% power conversion efficiency. *Nature materials* **17**, 820-826 (2018).

14 Liang, T. S. *et al.* A review of crystalline silicon bifacial photovoltaic performance characterisation and simulation. *Energy & Environmental Science* **12**, 116-148 (2019).

15 Asadpour, R., Chavali, R. V., Ryyan Khan, M. & Alam, M. A. Bifacial Si heterojunction-perovskite organic-inorganic tandem to produce highly efficient (η T*∼ 33%) solar cell. *Applied Physics Letters* **106**, 243902 (2015).

16 Onno, A. *et al.* Predicted Power Output of Silicon-Based Bifacial Tandem Photovoltaic Systems. *Joule* (2020).

17 Dupré, O. *et al.* Design Rules to Fully Benefit From Bifaciality in Two-Terminal Perovskite/Silicon Tandem Solar Cells. *IEEE Journal of Photovoltaics* **10**, 714-721 (2020).

18 Geerligs, L. J., Zhang, D., Janssen, G. J. M. & Luxembourg, S. L. 4-terminal and 2-terminal tandem modules in bifacial operation: model analysis and comparison. doi:urn:NBN:nl:ui:24-uuid:a06611b9-78b2-46dd-8a04-ca02cac50111 (2018).
19 Coletti, G. *et al.* Bifacial Four-Terminal Perovskite/Silicon Tandem Solar Cells and Modules. *ACS Energy Letters* **5**, 1676-1680, doi:10.1021/acsenergylett.0c00682 (2020).
20 Onno, A., Chen, C., Koswatta, P., Boccard, M. & Holman, Z. C. Passivation, conductivity, and selectivity in solar cell contacts: Concepts and simulations based on a unified partial-resistances framework. *Journal of Applied Physics* **126**, 183103 (2019).
21 Lehr, J. *et al.* Energy yield modelling of perovskite/silicon two-terminal tandem PV modules with flat and textured interfaces. *Sustainable Energy & Fuels* **2**, 2754-2761 (2018).
22 Lehr, J. *et al.* Energy yield of bifacial textured perovskite/silicon tandem photovoltaic modules. *Solar Energy Materials and Solar Cells* **208**, 110367 (2020).
23 Jacobs, D. A. *et al.* Light Management: A Key Concept in High-Efficiency Perovskite/Silicon Tandem Photovoltaics. *The journal of physical chemistry letters* **10**, 3159-3170 (2019).
24 Gharibzadeh, S. *et al.* Record Open-Circuit Voltage Wide-Bandgap Perovskite Solar Cells Utilizing 2D/3D Perovskite Heterostructure. *Advanced Energy Materials* **9**, 1803699 (2019).
25 Hoke, E. T. *et al.* Reversible photo-induced trap formation in mixed-halide hybrid perovskites for photovoltaics. *Chemical Science* **6**, 613-617 (2015).
26 Boccard, M. & Ballif, C. Influence of the Subcell Properties on the Fill Factor of Two-Terminal Perovskite–Silicon Tandem Solar Cells. *ACS Energy Letters* **5**, 1077-1082 (2020).
27 Köhnen, E. *et al.* Highly efficient monolithic perovskite silicon tandem solar cells: analyzing the influence of current mismatch on device performance. *Sustainable Energy & Fuels* **3**, 1995-2005 (2019).
28 Bush, K. A. *et al.* 23.6%-efficient monolithic perovskite/silicon tandem solar cells with improved stability. *Nature Energy* **2**, 1-7 (2017).
29 Holman, Z. C. *et al.* Parasitic absorption in the rear reflector of a silicon solar cell: Simulation and measurement of the sub-bandgap reflectance for common dielectric/metal reflectors. *Solar energy materials and solar cells* **120**, 426-430 (2014).
30 Liu, H. *et al.* A Worldwide Theoretical Comparison of Outdoor Potential for Various Silicon-Based Tandem Module Architecture. *Cell Reports Physical Science*, 100037 (2020).
31 Guerrero-Lemus, R., Vega, R., Kim, T., Kimm, A. & Shephard, L. Bifacial solar photovoltaics–A technology review. *Renewable and sustainable energy reviews* **60**, 1533-1549 (2016).
32 Aydin, E. *et al.* Room-Temperature-Sputtered Nanocrystalline Nickel Oxide as Hole Transport Layer for p–i–n Perovskite Solar Cells. **1**, 6227-6233 (2018).
33 Zhan, T., Xiong, J., Lee, Y.-H., Chen, R. & Wu, S.-T. Fabrication of Pancharatnam-Berry phase optical elements with highly stable polarization holography. *Optics express* **27**, 2632-2642 (2019).
34 Baker-Finch, S. C. & McIntosh, K. R. Reflection of normally incident light from silicon solar cells with pyramidal texture. *Progress in Photovoltaics: Research and Applications* **19**, 406-416 (2011).
35 Wilcox, S. & Marion, W. Users manual for TMY3 data sets. (2008).
36 Gueymard, C. A. Parameterized transmittance model for direct beam and circumsolar spectral irradiance. *Solar Energy* **71**, 325-346 (2001).
37 Schmager, R. *et al.* Methodology of energy yield modelling of perovskite-based multi-junction photovoltaics. *Optics express* **27**, A507-A523 (2019).
38 Baldridge, A. M., Hook, S., Grove, C. & Rivera, G. The ASTER spectral library version 2.0. *Remote Sensing of Environment* **113**, 711-715 (2009).